

## Dynamically consistent parameterization of mesoscale eddies. Part III: Deterministic approach

Pavel Berloff

Department of Mathematics, Imperial College London, Huxley Bldg., London SW7 2AZ, United Kingdom



### ABSTRACT

This work continues development of dynamically consistent parameterizations for representing mesoscale eddy effects in non-eddy-resolving and eddy-permitting ocean circulation models and focuses on the classical double-gyre problem, in which the main dynamic eddy effects maintain eastward jet extension of the western boundary currents and its adjacent recirculation zones via eddy backscatter mechanism. Despite its fundamental importance, this mechanism remains poorly understood, and in this paper we, first, study it and, then, propose and test its novel parameterization.

We start by decomposing the reference eddy-resolving flow solution into the large-scale and eddy components defined by spatial filtering, rather than by the Reynolds decomposition. Next, we find that the eastward jet and its recirculations are robustly present not only in the large-scale flow itself, but also in the rectified time-mean eddies, and in the transient rectified eddy component, which consists of highly anisotropic ribbons of the opposite-sign potential vorticity anomalies straddling the instantaneous eastward jet core and being responsible for its continuous amplification. The transient rectified component is separated from the flow by a novel remapping method. We hypothesize that the above three components of the eastward jet are ultimately driven by the small-scale transient eddy forcing via the eddy backscatter mechanism, rather than by the mean eddy forcing and large-scale nonlinearities. We verify this hypothesis by progressively turning down the backscatter and observing the induced flow anomalies.

The backscatter analysis leads us to formulating the key eddy parameterization hypothesis: in an eddy-permitting model at least partially resolved eddy backscatter can be significantly amplified to improve the flow solution. Such amplification is a simple and novel eddy parameterization framework implemented here in terms of local, deterministic flow roughening controlled by single parameter. We test the parameterization skills in a hierarchy of non-eddy-resolving and eddy-permitting modifications of the original model and demonstrate, that indeed it can be highly efficient for restoring the eastward jet extension and its adjacent recirculation zones.

The new deterministic parameterization framework not only combines remarkable simplicity with good performance but also is dynamically transparent, therefore, it provides a powerful alternative to the common eddy diffusion and emerging stochastic parameterizations.

### 1. Introduction

Importance of oceanic mesoscale eddies in maintaining general circulation of the global ocean is well-established [McWilliams \(2008\)](#). In ocean general circulation models (OGCMs), the most accurate accounting for the eddy effects is by resolving them dynamically. This brute-force approach requires the models to have nominal horizontal grid resolution of about 1 km, which is not feasible for many applications, including the Earth system and climate modelling studies that need long-time simulations of the global ocean. Thus, practical considerations require that the eddy effects have to be parameterized by

simple mathematical models embedded in non-eddy-resolving or eddy-permitting OGCMs. Searching for accurate and practical eddy parameterizations is a subject of ongoing and vigorous research, that also advances our theoretical understanding of the eddy dynamics and eddy/large-scale flow interactions.

There are several modern approaches to the eddy parameterization problem. Eddy diffusion is by far the most popular approach, due to its mathematical simplicity, long history, and many successes. The central idea of the eddy diffusion is making use of flux-gradient relations between nonlinear eddy fluxes and large-scale gradients of various material properties. If a flux-gradient relation is negative, in the sense that

E-mail address: [p.berloff@imperial.ac.uk](mailto:p.berloff@imperial.ac.uk).

eddies flux the property of interest down its gradient, then the parameterization can be formulated as the corresponding diffusion<sup>1</sup> law. For example, eddy diffusion of momentum (i.e., eddy viscosity) is implemented in all OGCMs, and implementation of eddy diffusion of isopycnal thickness (Gent and McWilliams (1990)) is one of the main parameterization success stories. Despite being physically consistent and useful in many situations, the diffusion approach contains the following two main problems. First, components of the diffusivity (tensor) coefficient are very inhomogeneous in space, and there is no clear scale separation between the eddies and large-scale flow in the key regions. This makes it difficult to estimate the diffusivity in practice and to relate it to the corresponding large-scale properties for ultimate closure. Second, in many circumstances the diffusivity coefficient is negative (e.g., in the “negative viscosity” situation; Starr (1968)), which makes the whole diffusion parameterization mathematically ill-posed and practically useless.

Ongoing research on eddy diffusion involves the following aspects: proposing different forms of the eddy diffusivity tensor (e.g., Smagorinsky, 1963; Gent and McWilliams, 1990; Zhao and Vallis, 2008; Jansen et al., 2015), diffusing different fields (e.g., Ringler and Gent, 2011; Ivchenko et al., 2014b), constraining eddy diffusivity (e.g., Eden and Greatbatch, 2008; Ivchenko et al., 2014a; Mak et al., 2017), estimating eddy diffusivity from the large-scale flow information (e.g., Visbeck et al., 1997; Killworth, 1997; Eden, 2011; Chen et al., 2015) and Lagrangian observations (e.g., Rypina et al., 2012). Finally, using non-Newtonian stress tensors, rather than flux-gradient relations, to represent eddy momentum fluxes can be viewed as a far extension of the eddy diffusion approach (Anstey and Zanna, 2017).

All alternatives to the eddy diffusion approach combined make up a smaller body of literature. Some of them are mentioned below, because of their novelty and relevance to the present work. The main motivation for the alternatives is inability of the diffusion model to account for nondiffusive effects of eddy fluxes, and the other motivation comes from practical difficulties in estimating eddy diffusivities. An emerging approach is to model eddy effects stochastically (e.g., Herring, 1996; Berloff and McWilliams, 2003; Berloff, 2005b; Duan and Nadiga, 2007; Frederiksen et al., 2012; Porta Mana and Zanna, 2014; Jansen and Held, 2014; Zanna et al., 2017), as justified by highly transient and structurally complicated patterns of the actual eddy flux divergences (e.g., Berloff, 2005a; Li and von Storch, 2013; Berloff, 2016). The main problems of this approach are in (i) providing physical constraints, as well as in (ii) determining stochastic-model parameters and (iii) relating them to the large-scale flow properties, but even tentative application of the approach to the oceanic component of a global climate model improves its simulations (Williams et al., 2016). A cross-breed between eddy diffusion and stochastic parameterization is the idea of adding randomness to the diffusivity coefficient in process studies (Berloff and McWilliams, 2003; Grooms, 2016) and comprehensive models (e.g., Buizza et al., 1999; Andrejczuk et al., 2016; Juricke et al., 2017). To summarize, the emerging stochastic parameterization approaches are promising, but the remaining challenges are serious.

A promising eddy parameterization idea is to employ the governing dynamics much better by solving explicitly (and even once) some intermediate-complexity dynamical model (e.g., locally fitted quasi-linear model) of the eddy effects (e.g., Grooms et al., 2015a; Berloff, 2015; Berloff, 2016). This approach allows us to model eddy flux divergence directly, instead of estimating it from the large-scale gradient and eddy diffusivity, although the diffusivity, as well as the eddy fluxes, can be also estimated from it (Berloff, 2016). Another set of eddy parameterization ideas, which are directly related to the subject of this paper, involves proactive roughening of the resolved flow field (San et al., 2013; Porta Mana and Zanna, 2014; Zanna et al., 2017). We emphasize these studies, because our results show that proper

roughening helps to restore the eddy backscatter mechanism, which is in our focus, and, thus, helps to parameterize the eddies.

The goal of this paper is to provide arguments supporting the key eddy backscatter mechanism and to demonstrate that, in situations when this mechanism is poorly resolved, it can be invigorated by roughening the eddy field. The paper is organized as the following. In the next section we outline the double-gyre ocean model; then, in Section 3 we provide statistical analysis of the reference flow solution, which is scale-aware decomposed in terms of its large-scale and eddy components, and identify rectified contributions of the eddies to the large-scale circulation. In Section 4 we demonstrate, by progressively suppressing the eddy scales, that most of the nonlinear part of the reference flow solution, and especially the eastward jet extension of the western boundary currents and its adjacent recirculation zones, owes its existence to the backscatter of the eddy scales. This analysis leads us to the hypothesis, that straightforward amplification of the eddy scales in eddy-permitting (but not properly eddy-resolving) ocean models can restore the missing eddy backscatter and, thus, parameterize effects of the unresolved eddies. In Section 5 we systematically confirm this hypothesis by parameterizing and progressively restoring eddy backscatter in a hierarchy of eddy-permitting models, and by demonstrating substantial improvements of the model solutions. Thus, the parameterization framework is found suitable for broad range of eddy-permitting models and spatial grids. Finally, we discuss the results in the concluding Section 6.

## 2. Ocean model

The dynamical model and its reference solution are discussed in Parts I and II (Berloff, 2015; 2016) of this work, therefore, we just remind that the focus is on the classical double-gyre quasigeostrophic (QG) potential vorticity (PV) model representing wind-driven mid-latitude ocean circulation. The model is configured in a flat-bottom square basin filled with 3 stacked isopycnal fluid layers and aligned with the usual zonal and meridional coordinates. The governing equations for the layered PV anomalies  $q_i$  and velocity stream functions  $\psi_i$  are

$$\frac{\partial q_1}{\partial t} + J(\psi_1, q_1) + \beta \frac{\partial \psi_1}{\partial x} = W + \nu \nabla^4 \psi_1, \quad (1)$$

$$\frac{\partial q_2}{\partial t} + J(\psi_2, q_2) + \beta \frac{\partial \psi_2}{\partial x} = \nu \nabla^4 \psi_2, \quad (2)$$

$$\frac{\partial q_3}{\partial t} + J(\psi_3, q_3) + \beta \frac{\partial \psi_3}{\partial x} = -\gamma \nabla^2 \psi_3 + \nu \nabla^4 \psi_3, \quad (3)$$

$$q_1 = \nabla^2 \psi_1 + S_1 (\psi_2 - \psi_1), \quad (4)$$

$$q_2 = \nabla^2 \psi_2 + S_{21} (\psi_1 - \psi_2) + S_{22} (\psi_3 - \psi_2), \quad (5)$$

$$q_3 = \nabla^2 \psi_3 + S_3 (\psi_2 - \psi_3), \quad (6)$$

where the layer index starts from the top, and  $J(, )$  is the Jacobian operator. The basin size is  $L = 3840$  km, the layer depths are  $H_1 = 250$ ,  $H_2 = 750$ , and  $H_3 = 3000$  m;  $\beta = 2 \times 10^{-11} \text{ m}^{-1} \text{ s}^{-1}$  is the planetary vorticity gradient;  $\nu = 20 \text{ m}^2 \text{ s}^{-1}$  is the eddy viscosity;  $\gamma = 4 \times 10^{-8} \text{ s}^{-1}$  is the bottom friction; the stratification parameters  $S_1$ ,  $S_{21}$ ,  $S_{22}$  and  $S_3$  are chosen so, that the first and second Rossby deformation radii are  $Rd_1 = 40$  km and  $Rd_2 = 20.6$  km, respectively; and  $W(x, y)$  is the asymmetric double-gyre wind forcing. The layer-wise model equations, augmented with the partial-slip lateral-boundary conditions and mass conservation constraints, are solved numerically on the uniform  $513^2$  grid with 7.5 km nominal resolution.

The flow solution is numerically converged, and the flow regime remains qualitatively similar even at much lower values of the eddy viscosity  $\nu$ , although its quantitative characteristics keep changing and show no convergence over the explored range of  $\nu$  (Shevchenko and

<sup>1</sup> Extension to hyperdiffusion can be done by considering gradient cubed.

Berloff 2015). The model is spun up from the state of rest, until the full statistical equilibration is reached; then, it is run for 2700 years, with the solution saved every 10 days. Only 110 years of the solution record are used for analyses of this paper, and we checked that doubling the record yields no significant changes of the reported statistics.

### 3. Analysis of the reference flow solution

This section discusses decomposition of the flow and its main components, and provides further statistical analyses and interpretations.

#### 3.1. Scale-aware decomposition of the flow

All model solutions are routinely decomposed into the large-scale and eddy (small-scale) flow components by running simple moving-average spatial filter over the PV anomaly field in each isopycnal layer. The large-scale and eddy velocity stream functions are obtained by the elliptic inversion (4)–(6) of their corresponding PV anomaly fields. The spatial filter is a square aligned with the basin and with the size of  $5Rd_1$ , which is roughly the scale of baroclinic eddies. In the vicinity of the lateral boundaries, we limited the filter half-size to the shortest distance from the reference point to the boundary. We checked that modest variations of the filter size (by  $\pm Rd_1$ ) yield no significant changes in the results. The large-scale flow component is denoted by angular brackets, e.g.,  $\langle q_i \rangle$ , and the eddy component is denoted by prime, e.g.,  $q'_i$ . Each flow component or the full flow are also decomposed into the time mean denoted by overbar, e.g.,  $\overline{q}_i$ , and temporal fluctuation (or transient component) denoted by tilde, e.g.,  $\tilde{q}_i$ . The decomposition results in the upper and deep ocean are illustrated by Fig. 1 and discussed further below. Note, that the implemented scale-aware flow decomposition involves only spatial and no temporal filtering, therefore, it is fundamentally different from the classical Reynolds decomposition into the time mean and temporal fluctuations around it. Thus, we allow large-scale flow to evolve in response to the action of eddies, its own nonlinearity, and the linear terms, all of which can be diagnosed from the dynamics, provided availability of the decomposed flow components. Note, also, that the filtered eddies can be nominally “seen” on eddy-permitting grids, but their dynamical resolution can not be adequate.

The time-mean and instantaneous circulation snapshots (Fig. 1) illustrate the reference double-gyre flow solution with its well-developed eastward jet extension of the western boundary currents. The flow solution is characterized not only by vigorous eddy field (Fig. 1, right panels), but also by large-scale flow fluctuations (Fig. 1h,n) capturing the corresponding variability component of the eastward jet and its adjacent recirculation zones. This variability includes meandering of the jet, as well as meridional shifts of the jet axis and variations of the jet amplitude (Berloff et al., 2007). The upper-ocean, time-mean large-scale flow (Fig. 1b) contains roughly only about a third of the eastward jet and its recirculations, as we show further below, and the rest of the them is contained in the eddy field. The presence of a permanent large-scale statistical component in the eddy field may appear counter-intuitive, but only from perspective of the most common Reynolds flow decomposition in the time mean and fluctuations around it, and not from perspective of the employed scale-aware flow decomposition, which allows eddies to have nonzero time-mean part. In the transient upper-ocean eddy component  $\tilde{q}'_i$ , note a ribbon of the opposite-sign PV anomaly straddling the meandering eastward jet core (Fig. 1f,i) and present in each flow snapshot. This ribbon represents systematic amplification of the evolving jet that can be viewed as a transient pattern characterized by large spatial scales. It is identified here as a part of the eddy field, because the spatial scale-aware filter is isotropic and, therefore, does not take into account anisotropic nature of the eastward jet and its adjacent eddies. We argue that this pattern, referred to as *transient rectified eddies*, must be represented by OGCMs, at least in some

coarse-grained or averaged sense.

Let's now consider eddy forcing—an important quantity characterizing eddy effects—defined as

$$EF_i(t, x, y) \equiv -[\nabla \mathbf{u}_i \cdot \mathbf{q}_i - \nabla \langle \mathbf{u}_i \rangle \cdot \langle \mathbf{q}_i \rangle], \quad i = 1, 2, 3, \quad (7)$$

and dominated in the reference solution by its upper-ocean component  $EF_1(t, x, y)$ . The eddy forcing field consists of the time-mean  $\overline{EF}_i(x, y)$  and transient (i.e., fluctuation)  $\tilde{EF}'_i(t, x, y)$  components (not shown; see Berloff, 2016). The former component is a large-scale pattern, which enters the time-mean dynamical balance and, therefore, can be interpreted as the time-mean nonlinear eddy effect maintaining the time-mean flow anomaly. The latter component is dominated by much more intensive, small-scale fluctuations, that induce transient small- and large-scale flow anomalies but do not enter the time-mean dynamical balance directly. The indirect effect of  $\tilde{EF}'$  on the large-scale flow, including its time mean, is referred to as the *eddy backscatter*. Around the eastward jet extension, Berloff (2016) estimated covariances between the evolving large-scale PV anomaly and individually the time-mean and transient components of the eddy forcing and showed that although both covariances are positive, in the sense that each eddy forcing component contributes to maintaining the jet and its adjacent recirculation zones, the latter covariance is much larger, suggesting that the eddy backscatter is the most important driver of the jet and recirculations. This is, of course, a statistical argument, and in order to make a dynamical argument, one has to suppress the transient eddy forcing and find the corresponding consequences for the large-scale flow. In Sections 4 and 5, we actually provide the missing dynamical argument by showing that the backscatter can be suppressed/invigorated by damping/amplifying the small scales, and this action induces permanent large-scale flow anomalies. Proposed stochastic eddy parameterizations (Section 1) aim to stimulate the eddy backscatter by adding explicit stochastic forcing, whereas the main novelty of our approach is achieving the same goal deterministically.

#### 3.2. Jet-following remapping of the flow

In order to identify better and quantify the transient rectified eddy component, we developed and applied the novel method of remapping the double-gyre flow into the time-dependent curvilinear coordinate system, which follows the eastward jet core. In fact, the main purpose of the whole remapping is to transform the transient rectified eddy PV anomaly into the permanent anomaly, and, thus, to make it explicit and argue that some fraction of the eddy field should be interpreted as part of the large-scale flow component. This interpretation is pattern-wise and not dynamical, because the eddies still act on the large-scale flow via eddy forcing and backscatter mechanism — this will be demonstrated by damping the eddies and monitoring the induced effect on the large-scale flow.

The remapping method is somewhat similar to the “jet reference frame” method developed by Delman et al. (2015) for use in primitive-equation models, but there are also significant differences discussed further below. Other methods for detecting jets are discussed by Chapman (2014), and our approach is within the contour-type methods. Overall, statistics of the remapped flow is like statistics taken following the jet, and it is qualitatively different from the statistics taken within the Eulerian framework (e.g., David et al., 2017).

The remapping method algorithm starts by searching for the evolving eastward jet axis in each instantaneous flow snapshot. We define the evolving jet axis by using information only from the combined time-mean and large-scale flow component, because complete information on transient eddies is not available in eddy-permitting circulation models. Hence, by construction transient eddy flow is allowed to cross the jet axis, but the rest of the flow is not allowed to do this. We focused the algorithm on the upper ocean in the rectangular subdomain defined by  $0.05L < x < 0.87L$  (near the western boundary the jet axis becomes

meridional, and in the eastern basin it is poorly defined and also turns meridional; hence, both regions are excluded) and  $0.45L < y < 0.65L$  (the jet axis is always contained within this region, as our analyses showed).

First, we defined the jet axis as the large-scale (plus time-mean eddies) streamline, that is the closest one to the zero isoline<sup>2</sup> of the upper-layer relative vorticity — this involved bi-linear interpolations of the gridded relative vorticity and stream function fields. The interpolated stream function is not exactly constant on the zero isoline of the relative vorticity, because of both jet core meandering and interpolation errors. We overcame this ambiguity by calculating the average stream function value along the zero relative-vorticity isoline, by finding the interpolated streamline with this value, and by defining it as the jet axis. The algorithm was occasionally contaminated by zero relative vorticity values located clearly far away from the jet core. We carefully avoided these contributions by counting only locations characterized by the flow speed more than  $0.4 \text{ m s}^{-1}$ , as supported by the argument that the jet core should be characterized by relatively fast flow.

The outcome is very good, as illustrated by application of the algorithm to the time-mean flow (Fig. 2), in the sense that the resulting jet axis streamline  $Y_{mean} = Y_{mean}(x)$  approximately follows the maximum speed of the jet core and is a single-valued function. To obtain the time evolution of the jet axis, we applied the same algorithm to each flow snapshot. The only extra problem here was that in some (less than 1%) flow snapshots the jet axis had multiple values associated with a strong looping meander of the jet. In this case we allowed for a discontinuity in  $Y_{inst} = Y_{inst}(x, t)$  defining the jet axis, thus, keeping the axis single-valued. We checked that exclusion of the discontinuous flow snapshots is not significant for the follow-up statistical analyses and conclusions.

The proposed algorithm is similar to Delman et al. (2015), who collocated a jet axis with the steepest gradient of the sea surface height, rather than with the zero isoline of the geostrophic relative vorticity. Attempting to optimize the algorithm, we tried to collocate the jet axis streamline with the steepest gradient of (i) the upper-ocean stream function (i.e., with the fastest velocity), which is proportional to dynamic pressure and serves as a proxy for the sea surface height (absent in our rigid-lid QG model), and (ii) the PV anomaly. Both of these alternatives turned out to be bad choices, because these gradients are often noticeably off the resulting jet core streamline.

Next, we remapped each snapshot of the PV anomaly fluctuation component by the continuous linear transformation (described further below) that maps:

$$\begin{aligned} Y_{inst}(x, t) &\longrightarrow Y_{mean}(x); & \tilde{q}(x, y, t) &\longrightarrow \langle Q \rangle(x, y, t); \\ \tilde{q}(x, y, t) &\longrightarrow Q'(x, y, t), \end{aligned} \quad (8)$$

where layer index is omitted,  $Q$  denotes remapped PV component, and its  $y$  variable is the remapped coordinate. Note, that the tilde symbol (describing transient fluctuations) is dropped for both  $Q$  components, because the remapped fields may have and, actually, do have the time-mean components.

The velocity stream functions of the resulting remapped flow components are obtained by the PV inversion (4)–(6). By construction the remapped flow has the eastward jet axis always coinciding with its time-mean position  $Y_{mean}(x)$ . The remapping is done in each layer, based on the upper-layer jet axis, and one by one for each longitude, that is, for each meridional row of the data grid points. Since the jet axis is found for  $0.05L < x < 0.75L$ , only in this band of longitudes the PV anomaly component is remapped uniquely from location  $y$  into location  $\hat{y}$ , and the other longitudes remain intact. For example, let's consider some  $x$  and two intervals  $0 < y < Y_{inst}$  and  $0 < y < Y_{mean}$ , which lay to the south of the instantaneous and time-mean jet axes, respectively. The applied linear transformation is

$$\hat{y} = \frac{Y_{mean}}{Y_{inst}} y, \quad (9)$$

so that the interval  $[0, Y_{inst}]$  is linearly mapped into the interval  $[0, Y_{mean}]$ . The resulting remapped PV component is scaled by the factor  $C = Y_{inst}/Y_{mean}$ , so that by construction remapping conserves total PV integral over the interval. The other interval, from the instantaneous jet axis to the northern boundary of the basin, is treated similarly.

The remapped flow may have and, actually, has nonzero time mean  $\bar{Q}(x, y) = \langle Q \rangle + \bar{Q}'$  that represents the transient rectified flow component (Fig. 3c). Note that this component of the flow is an inherent part of the transient flow field, dominated by the eddies but also including some part of the large-scale flow fluctuations, and the remapping allowed us to extract it by straightforward time averaging. Similarly, we remapped the evolving eddy forcing field and found, that it is positively and strongly correlated with  $\bar{Q}(x, y)$ , which is consistent with the eddy backscatter amplifying the eastward jet and its adjacent recirculation zones.

Now, let's discuss systematically all components of the large-scale flow and illustrate them with Fig. 3. Since most of the gyres are in approximately linear (Sverdrup) balance, our starting point will be the linear solution (Fig. 3A) obtained by time integration of the linearized, eddy-resolving model with the reference parameters: the resulting solution contains very weak basin modes, therefore we show its time average. The linear solution is characterized by the gyres, very thin viscous western boundary layers and, most importantly, by complete absence of the eastward jet and its recirculations, which confirms that these features are fundamentally nonlinear phenomena. On the top of the linear solution, the flow nonlinearity is responsible for generation of the following time-mean flow components (Fig. 3a–c). First, there is the large-scale time-mean component, which contains about roughly one third of the eastward jet and also the counter-rotating gyre anomalies discovered by Shevchenko and Berloff (2016) and not fully explained. Second, there is the time-mean eddy anomaly, and, third, there is the transient flow anomaly illuminated by the flow remapping. All these flow components can be successively added up (Fig. 3d–f) to show their relative contributions. If the eddy backscatter hypothesis is correct, then the first component is maintained by the transient eddy forcing, and if the eddies are damped out, it will also disappear.

To summarize, in this section we decomposed the reference flow solution into the large-scale and eddy components and found that the former captures not only the mean gyres but also significant part of the eastward jet, as well as its large-scale variability. The eddy component also contains significant part of the time-mean eastward jet and its adjacent recirculation zones. The transient part of the eddy component contains not only isotropic small-scale variations of PV anomaly, but also highly anisotropic ribbons of the opposite-sign PV anomalies straddling the instantaneous eastward jet core and responsible for its systematic amplification. These PV anomalies can be interpreted as time-dependent adjacent recirculation zones and viewed as an important part of the circulation that in some coarse-grained or averaged sense needs to be simulated explicitly in a model, which does not completely resolve the eddies. To make the time-dependent adjacent recirculation zones explicit, we remapped the flow into the new, eastward-jet-following coordinate system and found, that the resulting flow anomaly is as significant as the time-mean eddy component. Because of their large-scale sizes, both of these components can be nominally resolved on a practical and even non-eddy-resolving grid, therefore, we refer to them as *rectified eddy component* of the circulation.

What does this mean from the eddy parameterization point of view? First of all, any parameterization has to be such, that not only the large-scale flow itself but also the rectified eddy component is explicitly simulated by the underlying model. What part of the eddy forcing do we have to parameterize in order to achieve this? May the time-mean eddy forcing be interpreted and modelled as just a small residual average of the actual eddy forcing? If a parameterization represents only time-

<sup>2</sup> This would be the perfect definition for a parallel-shear-flow jet with single velocity maximum.

mean part of the eddy forcing, it is doomed to miss the time-dependent adjacent recirculation zones, therefore, it is likely to misrepresent the whole dynamics and the actual circulation pattern (Berloff, 2005a; 2005b). Our working hypothesis is that the parameterization has to simulate the transient, rather than the time-mean, part of the eddy forcing, and this can efficiently restore the eddy backscatter that amplifies the eastward jet and its adjacent recirculation zones. In the next section we verify this hypothesis.

#### 4. Suppression of the eddy backscatter

In this section we suppress the eddy forcing dominated by its transient part by selectively damping the eddy scales, and demonstrate that this suppresses the eastward jet and its adjacent recirculation zones.

Commonly used analysis of the time-mean dynamical balance is not helpful here for at least two reasons. First, the time-mean balance does not tell us how exactly the time-mean eddy forcing relates to the transient eddy dynamics. Also, it is important to remember that the

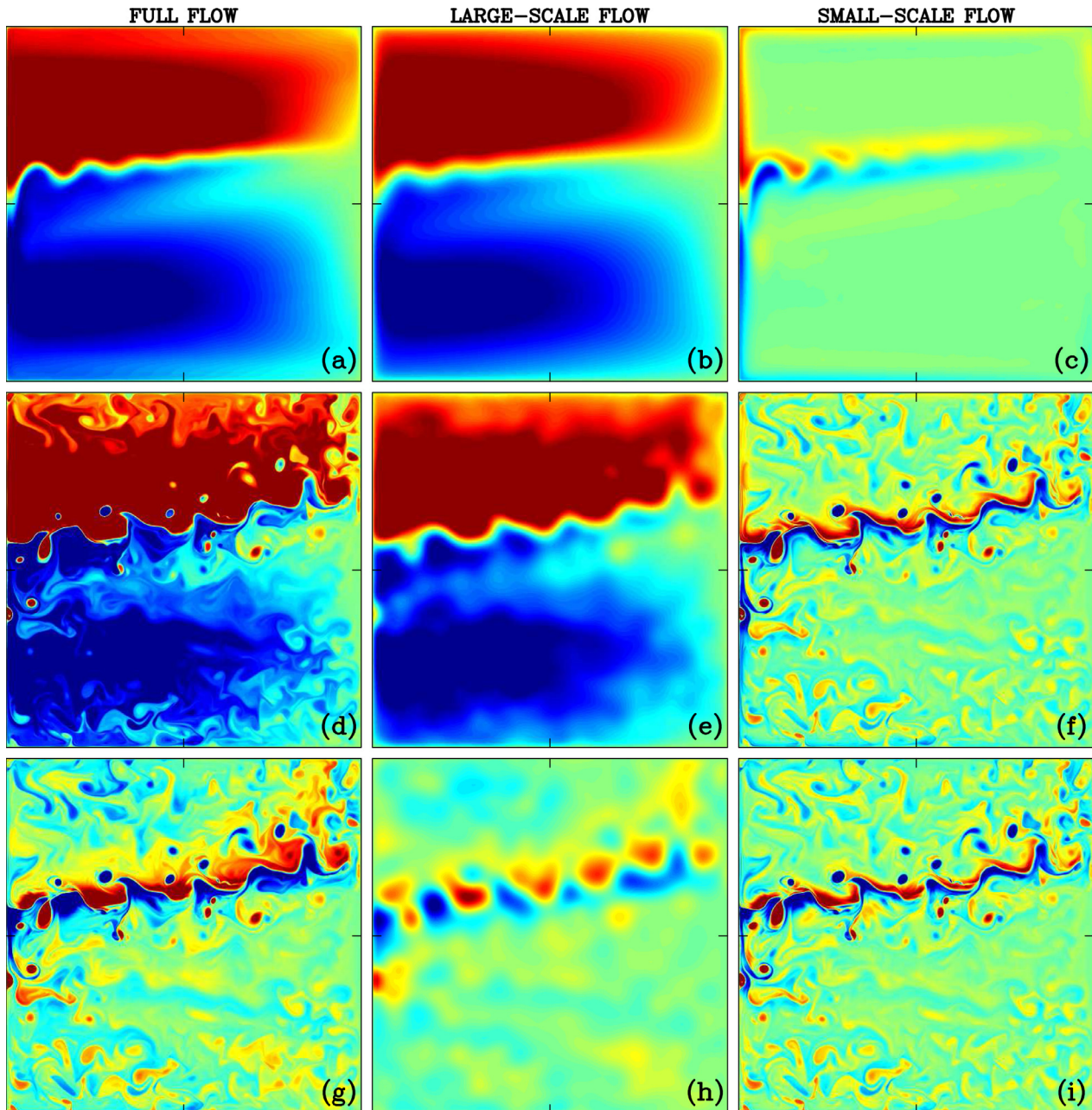


**Fig. 1.** Illustration of the reference eddy-resolving solution and its scale-aware decomposition. Shown are PV anomalies in the (a–i) upper, (j–l) middle, and (m–o) deep isopycnal layers; left, middle and right columns of panels show full, large-scale and small-scale (eddy) flows and their components, respectively. Upper-ocean circulation: (a–c) time-mean components, (d–f) instantaneous full flows corresponding to the same snapshot, (g–h) transient fluctuation components corresponding to the same snapshot; note, that flow in each middle panel is the sum of flows shown in the panels above (i.e., time mean) and below it (i.e., fluctuation). Flow fields in panels (a–i) have the same but arbitrary units, and the units in panels (j–l) and (m–o) are 4 and 10 times smaller, respectively. Note, that the large-scale flow contains basin-scale gyres and part of the eastward jet with its adjacent recirculation zones; eddies in the upper ocean are dominated by the ribbon of opposite-sign PV anomaly straddling the eastward jet; eddies in the middle layer cluster in quasi-zonal eddy striations populating westward return flows of the gyres (i.e., the northern and southern parts of the domain); eddies in the deep layer are most equally distributed around the basin.

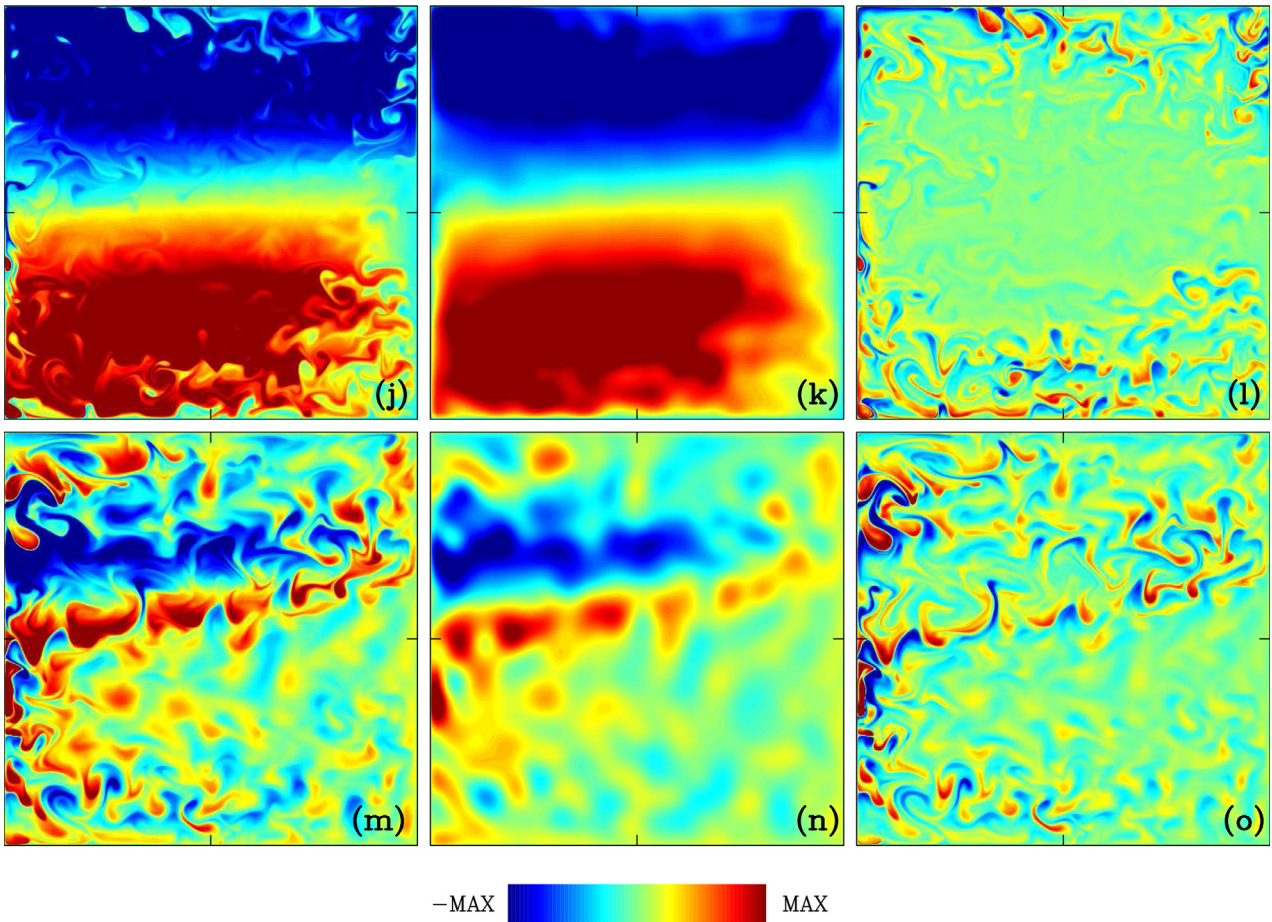


Fig. 1. (continued)

time-mean flow state is somewhat irrelevant, because it is actually never achieved, since the flow is significantly time-dependent (Sections 3.1 and 3.2). Attempts to simulate the time-mean flow in a reduced model incorporating only time-mean eddy forcing have failed, because the time-mean balance is not a stable steady state, and the prognostically modeled flow rapidly becomes time-dependent and produces its own nonlinear dynamical response (Berloff, 2005a). Second, there is a statistical argument (Berloff, 2016) that covariance of the transient eddy forcing with the large-scale PV anomaly in the eastward jet region is more than  $10^4$  times larger than the corresponding covariance of the time-mean eddy forcing, hence, shifting the focus away from the latter is statistically justified.

The above arguments are suggestive, but in order to nail down the issue and show directly, to what extent the small-scale transient eddies are responsible for maintaining the eastward jet, we implemented a direct, deterministic suppression of the small scales around the eastward jet and studied how the dynamical flow responses depend on the degree of suppression. Note, that in these simulations we kept intact all ocean model parameters and spatial grid resolution, so that the outcome is not contaminated by the numerical resolution errors, larger eddy viscosity and numerical convergence issues, as it would be in case of a coarse-gridded version of the model. Why did we decide to damp the eddies rather than the eddy forcing, which is available on the fine grid? This is because the latter, being a highly differentiated quantity, can not be adequately estimated in eddy-permitting models, which are in the focus of the proposed parameterization framework. To strengthen our conclusions, we also ran supplementary simulations with coarse-gridded versions of the ocean model, that do not resolve the smallest scales and misrepresent dynamics of the partially resolved small scales. These simulations, by providing alternative and practically most

relevant take on the problem, confirm our earlier conclusions, that the eastward jet extension and its adjacent recirculation zones are driven primarily by the eddy backscatter, rather than by the larger-scale nonlinear interactions.

Implementation of the algorithm is straightforward. The small-scale (eddy) damping is confined to the rectangular region containing the eastward jet (Section 3.2) and (formulated as the following. First, we interactively apply our spatial filter (Section 3) to each layer and separate the eddy component; second, we damp it according to

$$\frac{\partial q'}{\partial t} = -\frac{q'}{T}, \tag{10}$$

where  $T$  is the variable damping-time parameter, and layer index is omitted. Since, by construction the damping does not affect the large scales, that is,  $\partial \langle q \rangle / \partial t = 0$ , and also  $q = \langle q \rangle + q'$ , we can write:

$$\frac{\partial (q - \langle q \rangle)}{\partial t} = -\frac{q - \langle q \rangle}{T} \rightarrow \frac{\partial q}{\partial t} = -\frac{q - \langle q \rangle}{T}, \tag{11}$$

so that the rhs term can be added to the governing Eqs. (1)–(3). By discretizing with the Euler time stepping and introducing  $\epsilon = \Delta t / T$ , the damping term is implemented on each new time step as the PV anomaly update:

$$q_{n+1} = q_n - \epsilon (q_n - \langle q_n \rangle) \rightarrow q_{n+1} = \langle q_n \rangle + (1 - \epsilon)(q_n - \langle q_n \rangle). \tag{12}$$

Dependence of the flow solution on the damping-time parameter  $T$  is illustrated by Fig. 4, which shows that, as the eddies are gradually suppressed, the eastward jet and its recirculations gradually disappear from the solution. Thus, the eddy damping affects not only the eddies themselves, which is obvious, but also the large-scale component of the eastward jet. Without the backscatter the large-scale component would

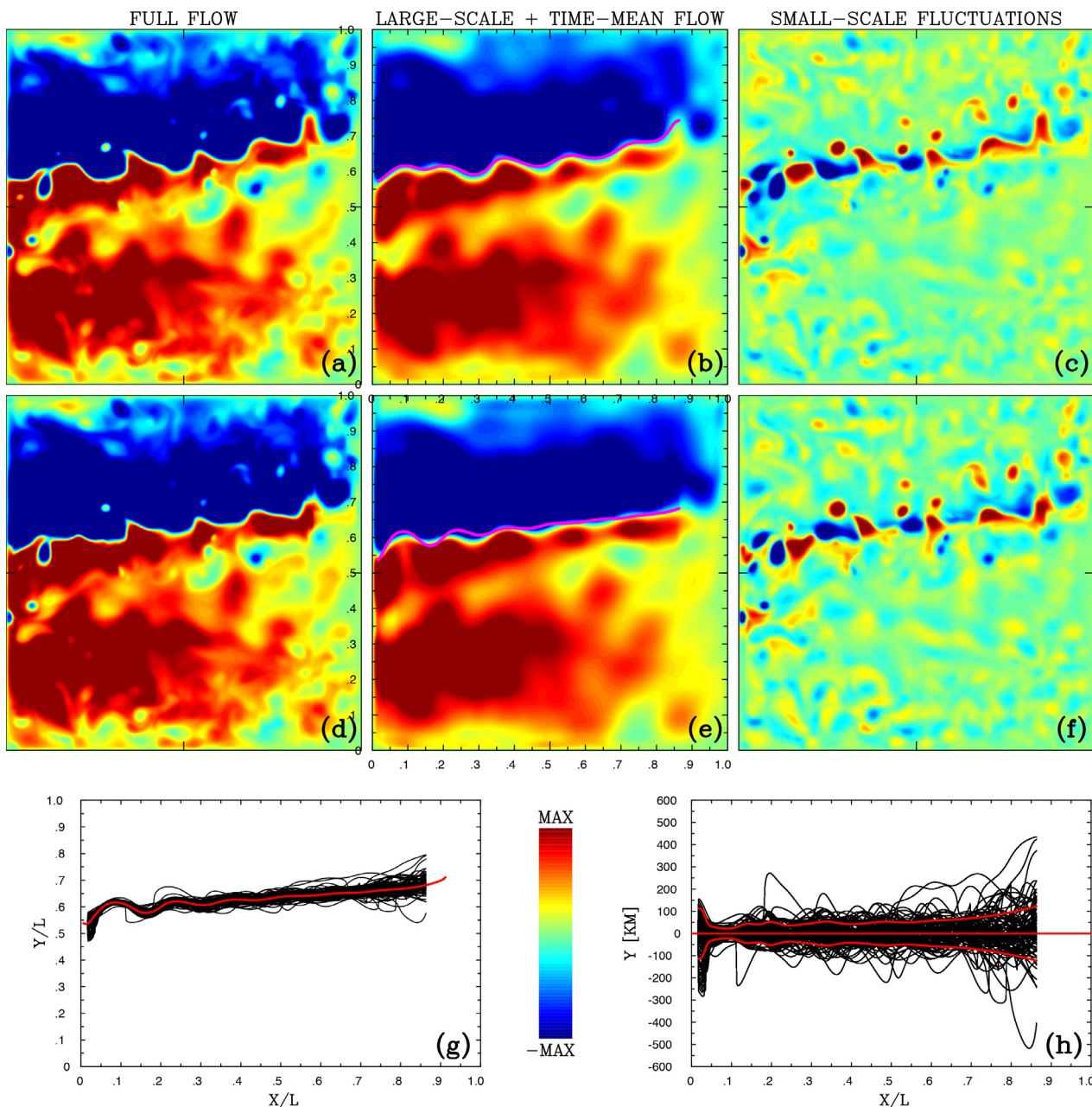
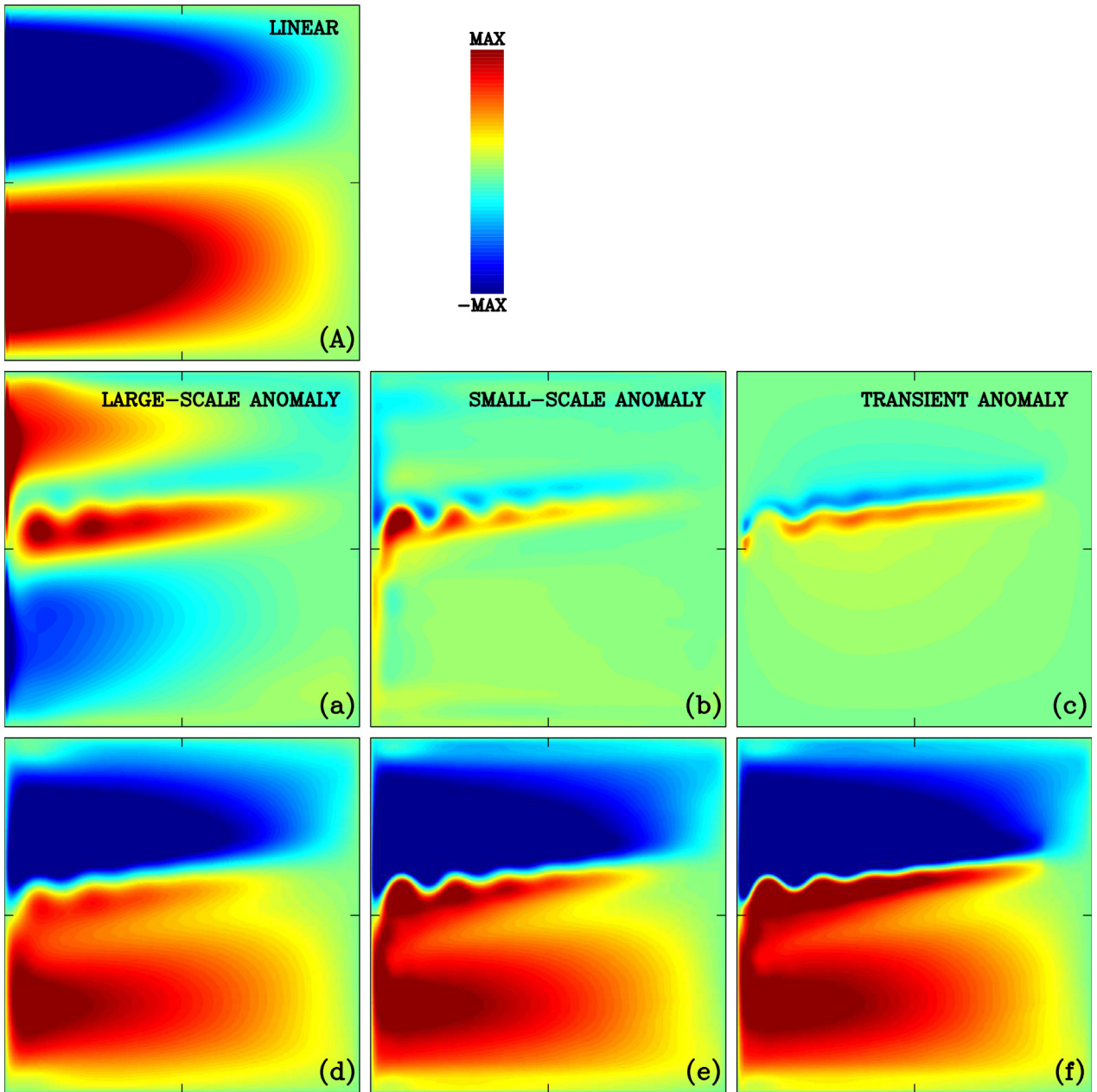


Fig. 2. Illustration of the eastward jet variability and action of the jet-following flow remapping. Upper row of panels shows an original flow snapshot in terms of the upper-ocean velocity streamfunction: (a) full flow, (b) combined large-scale plus time-mean flow component used for finding the eastward jet axis (indicated by the magenta curve), and (c) transient eddies. Middle row of panels shows remapped equivalents of the flows in the upper row of panels: (d) full flow, (e) combined large-scale plus time-mean flow component remapped so that the eastward jet axis coincides with its time-mean position (indicated by the magenta curve), and (f) remapped transient eddies. Note, that the remapping introduces visually small changes of the flow, nevertheless, as shown further below, it allows to filter out the rectified transient eddy anomalies. Flow fields have the same but arbitrary units, and the color scale is as in Fig. 1. Variability of the eastward jet axis is illustrated by the lower pair of panels: (g) superposition of instantaneous jet axes (black lines) around the time-mean jet axis (red line); and (h) zoomed in part of the domain with instantaneous jet axes plotted in terms of their differences from the time-mean jet axis (red lines indicate the time-mean jet axis and standard deviations around it. (For interpretation of the references to colour in this figure legend, the reader is referred to the web version of this article.)

be still maintained by the large-scale nonlinear interactions, but this is not the case. For example, the solution with  $T = 10$  days has no traces of the eastward jet extension and may even appear linear, but this is a misleading appearance (Fig. 4), because it contains the counter-rotating gyre anomalies (Shevchenko and Berloff, 2016), which are not only robustly present for all explored values of  $T$  but even noticeably increase with progressively damped eddies. As  $T$  increases, the backscatter acts more efficiently, and the eastward jet and its recirculations become more pronounced. The corresponding error  $E$ , formally defined as the L1-norm (i.e., spatial integral of the absolute value) of the upper-

ocean time-mean stream function anomaly induced by the damping, monotonically goes to zero as  $T \rightarrow \infty$ . It is tempting to change the sign of  $T$ , so that the damping reverses to amplification, while keeping its absolute value large, so that the resulting amplification is moderate. The outcome is such, that the eastward jet and its recirculations become amplified beyond their reference strength (Fig. 4m–o). This simple, unwarranted and important result suggests that an underestimated (e.g., by overdamping or underresolving) eddy backscatter can be amplified in a similar fashion — further development of this idea is in Section 5.



**Fig. 3.** Upper-ocean time-mean flow components induced by the nonlinearities. Shown are PV anomalies; the units are arbitrary but the same for all panels. (A) Linear flow solution; anomalies on the top of the linear solution and corresponding to (a) large-scale, (b) small-scale (eddy), and (c) rectified transient small-scale (eddy) components. Combined fields with the following added to the linear solution: (d) large-scale component; (e) large- and small-scale components; (f) all components (a–c). Note, that counter-rotating gyre anomalies are present only in the large-scale nonlinear component, whereas recirculations supporting the eastward jet are spread over all 3 nonlinear components.

Apparently, large-scale flow nonlinearities, which are not directly affected by the damping, can not compensate for the missing eddy backscatter. The eddy suppression works, because it counteracts the main feature of the eddy backscatter: systematic positive correlation between the eddy forcing and the evolving large-scale PV anomaly. This can be seen by taking the extra forcing given by rhs of (11) and multiplying it with  $q$ , which is the formally resolved field. The resulting product  $(-q^2 + q\langle q \rangle)/T$  should be integrated in space, in order to obtain the spatial covariance. The first term will be the autocovariance of  $q$ , whereas the second term will be always smaller in magnitude, because it corresponds to the cross-covariance of  $q$  with its smoother version. Hence, the extra forcing is always negatively correlated with the PV, and, therefore, acts against the eddy backscatter.

## 5. Amplification of the eddy backscatter: parameterization framework

Previous section showed that the eddy backscatter can be easily suppressed by suppressing the eddies, and this results in weakening and even elimination of the eastward jet extension and its adjacent recirculation zones. This leads us to formulating remarkably simple and powerful hypothesis with enormous practical potential: proactive amplification of the eddy backscatter can be achieved by undamping (i.e., roughening) eddy-scale spatial variability, and this process can parameterize the eddy effects up to the point, that the eastward jet extension and its adjacent recirculation zones can be simulated by an ocean circulation model lacking proper dynamical resolution of the eddy scales. In this section, we verify this hypothesis and systematically assess skills

of the proposed deterministic eddy parameterization within the QG double-gyre setting.

The eddy backscatter can be underestimated for one or both of the following reasons: it can be underresolved by the numerical grid or overdamped by excessive diffusion or friction. We are going to consider each of these factors independently, and there are the following

subtleties to deal with. One of them is that in practice grid resolutions are usually refined/coarsened by doubling/halving rather than gradually, and this makes establishing continuous dependencies on the resolution somewhat irrelevant. Next, effect of the resolution is always twofold: for example, a coarsening implies, on the one hand, that the smaller scales just disappear from the consideration, as they can not “be

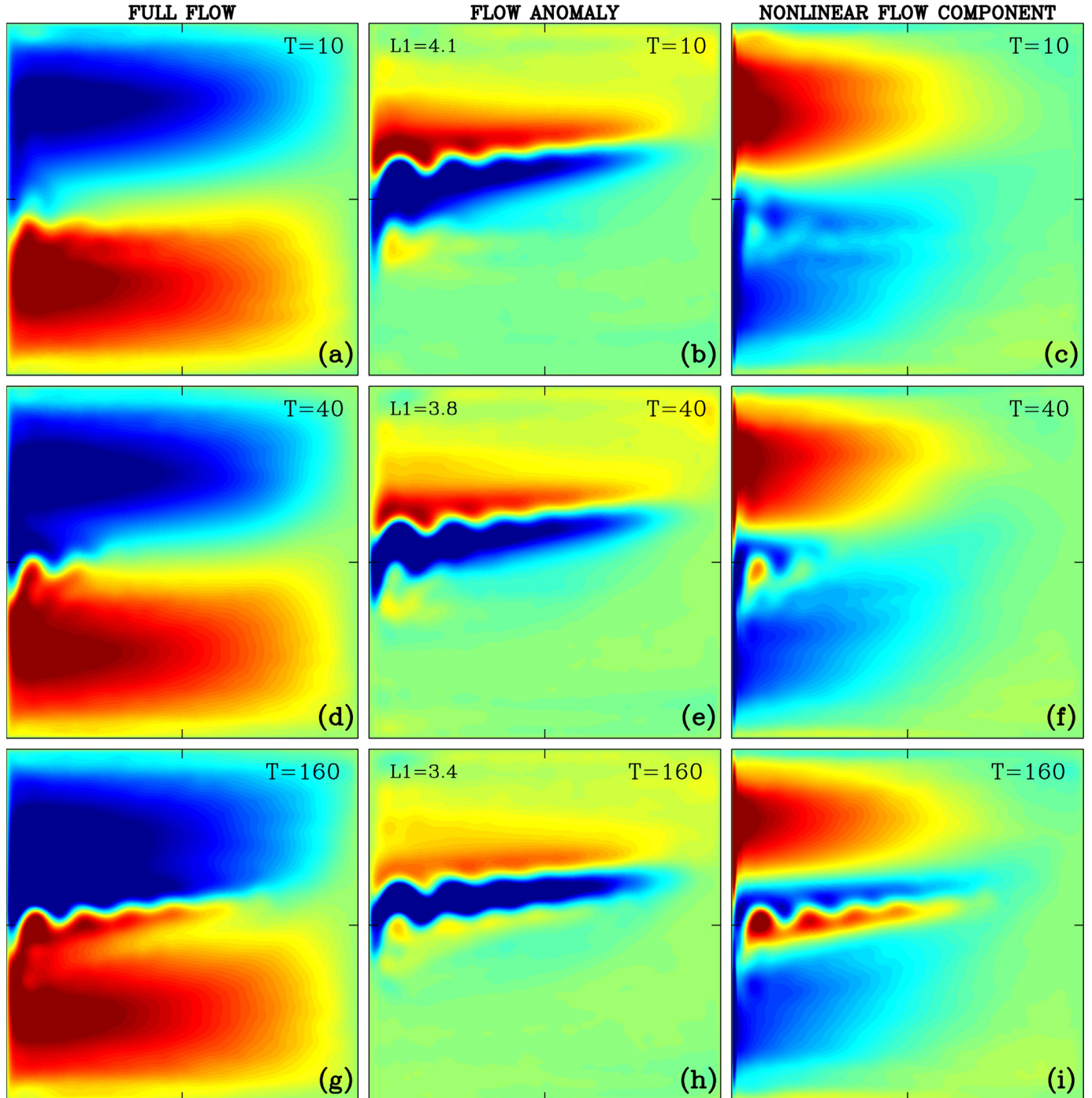


**Fig. 4.** Solution dependence on the damping time  $T$  parameter: (a–c)  $T = 10$ , (d–f)  $T = 40$ , (g–i)  $T = 160$ , (j–l)  $T = 640$ , (m–o) (negative damping)  $T = -280$  days. Shown flow fields are time-mean upper-ocean velocity stream functions, and the units are arbitrary but the same for all panels. Left panels show full flows; middle panels show flow anomalies described by the differences between the damped and reference solutions; and right panels show differences between the full flows (left panels) and the linear double gyres (Fig. 3A). Reference solution corresponding to  $T = \infty$  can be seen in Fig. 3f. Middle panels indicate  $L_1$ -norms of the corresponding fields averaged over the reference rectangular subdomain containing the eastward jet of the reference solution; each  $L_1$ -norm is divided by the  $L_1$ -norm corresponding to the solution for  $T = 640$  shown in panel (k); increasing value of the  $L_1$ -norm indicates the increasing flow anomaly. Note that damping of the backscatter gradually removes the eastward jet and its recirculations, and roughening (i.e., negative damping) of the backscatter has the opposite effect; the counter-rotating gyre anomalies remain largely intact by these processes.

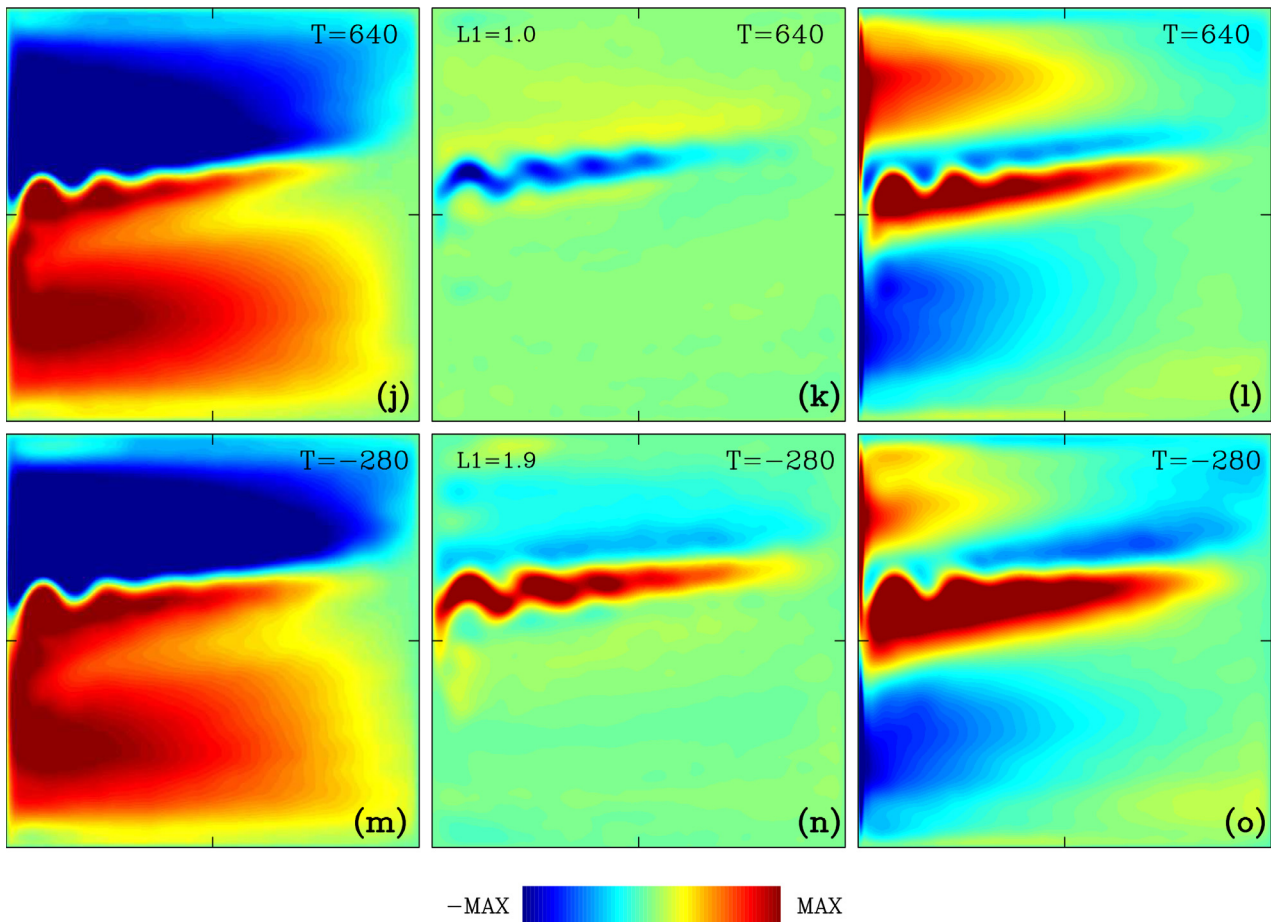


Fig. 4. (continued)

seen” by the grid, and, on the other hand, the numerical errors increase for all scales that are nominally represented by the coarsened grid. Finally, coarsening of the grid resolution is usually accompanied by substantial increase of the eddy viscosity and diffusivity coefficients, because the smaller eddy scales become dynamically unavailable and, thus, require a parameterization.

We are going to handle the situation by considering the parameterization implemented in two types of models. The first type is referred to as the “equivalent coarse-gridded model”, and the second type — as the “(common) coarse-gridded model”. In the former type of model, the nominal grid resolution (i.e.,  $513^2$ ) and the eddy viscosity are kept the same as in the reference eddy-resolving solution, thus, implying that neither numerical accuracy nor effect of the larger viscosity are in place, and the only acting effect is availability of the smaller scales feeding the backscatter. The smaller scales are removed by applying the spatial filter with the half width (here, chosen to be 15, 30 and 60 km) defining the “equivalent-grid” resolution, respectively, as  $257^2$ ,  $129^2$  and  $65^2$  (note, that in principle this resolution can be changed continuously) and aggressively damping everywhere in the basin all the resulting small scales with the variable damping time parameter values  $T_d = 5, 4, 3, 2$  and 1 day (further reduction of  $T_d$  results in insignificant effect on the solutions). In the latter type of model, which is conventional but mixes up all resolution effects, the grid resolution is successively halved to be  $257^2$ ,  $129^2$  and  $65^2$ , and the eddy viscosity is also increased, in order to keep the solutions numerically converged. Both model types have the eddy parameterization implemented (locally around the eastward jet, as in Section 4), but with negative values of  $T = T_a$  (here, subscript indicates amplification, in order to distinguish from  $T_d$ ), so that it amplifies the backscatter, being controlled by the only parameter  $T_a$  (its absolute values are quoted).

Quality of the parameterized solutions is systematically and objectively assessed by considering the flow anomalies between the parameterized and reference (i.e., “true” eddy-resolving) solutions and by comparing these anomalies with those differing the corresponding non-parameterized and reference solutions. In practice we focus on the upper-ocean velocity stream functions and consider L1-norms of the time-mean (here, 100 years time averaging was applied to statistically equilibrated solutions) anomalies in the subdomain with the reference eastward jet and its recirculation zones. The absolute error  $E$  obtained with the above metrics proved to be convenient and efficient for characterizing the main effect of the parameterization, as also backed up by visual inspections of the flow solutions.

Parameterization effect on the equivalent coarse-grid models is illustrated by Fig. 5 (dependencies of the absolute and relative errors on the equivalent resolution and  $T_a$ ) and Fig. 6 (typical time-mean circulations and flow anomalies). In the former figure the parameterized solution errors  $E$  are compared with the errors of the basic (i.e., non-parameterized) solutions  $E_b$ , and the relative errors  $E_{rel} = E/E_b$  are also shown for illustration. The main conclusion is that, on the eddy-permitting grids  $257^2$  and  $129^2$ , the parameterization largely restores the eastward jet and its recirculations, provided that the small-scale damping is not too large, which makes full sense, as the backscatter is driven by the small scales. Improvement on the coarsest, non-eddy-resolving  $65^2$  grid, which has grid interval 1.5 times larger than the first baroclinic Rossby radius, is more modest (about half of the jet and its recirculations restored) but still significant, suggesting that the applicability range for the proposed parameterization is remarkably wide. It follows from the main conclusion that keeping spatially nonuniform grid, with finer resolution in the eastward jet region, should be beneficial for the parameterized model performance. Second, we concluded

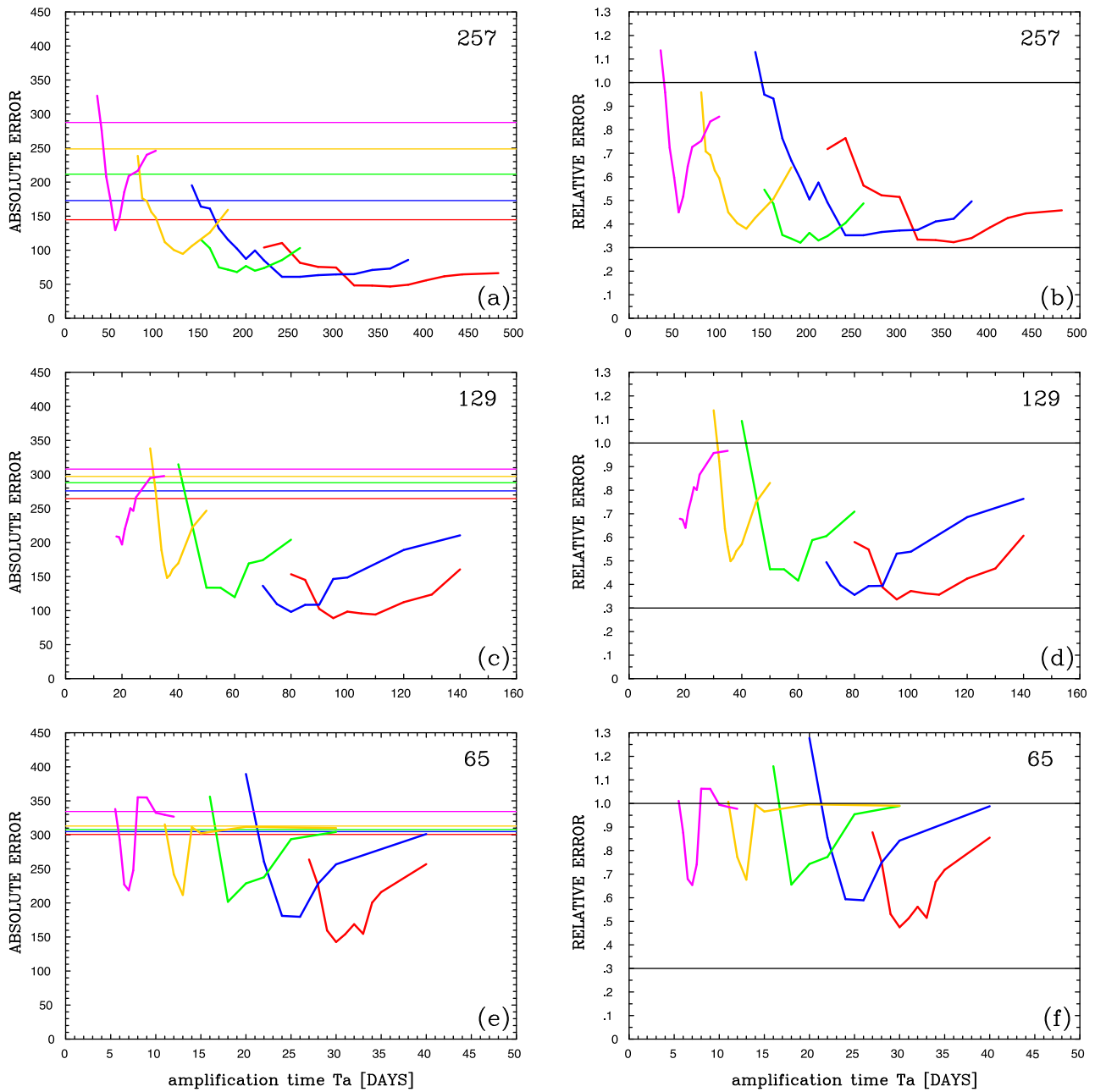


**Fig. 5.** Illustration demonstrating that the parameterization substantially improves the eddy-permitting model, and progressively more so for less damped and less coarsened basic solutions. Quality of the parameterized (by amplification of the backscatter) solutions with different equivalent grid resolutions (i.e., coarsenings) and damping rates. Equivalent grid sizes in terms of the grid points: (a,b)  $257^2$ , (c,d)  $129^2$ , (e,f)  $65^2$ . Colours correspond to the five basic solutions with the following damping times  $T_d$  (in days): 5 (red), 4 (blue), 3 (green), 2 (yellow), and 1 (magenta). Horizontal straight (coloured) lines on the left panels indicate errors  $E_b$  of the basic solutions; the larger is  $T_b$ , the smaller is the error (and the lower is the corresponding line); all errors are given in terms of (arbitrary) nondimensional units, which are the same for all left panels. Curved (coloured) lines on the left panels show errors  $E$  of the parameterized (i.e., amplified) basic solutions, as functions of the amplification time  $T_a$ . Right panels show the corresponding relative error  $E_{rel} = E/E_b$  curves, with all values normalized by the basic-solution error (i.e., the lower is the curve, the more is the improvement by the parameterization); for convenience, the black horizontal lines indicate  $E_{rel}$  equal to unity and 0.3. (For interpretation of the references to colour in this figure legend, the reader is referred to the web version of this article.)

that for each model setting there is an optimal range of the control parameter  $T_a$ , which is of the order of months. This range is broader for finer resolution and weaker damping rates, and in practice it should be calibrated by the eddy energy (e.g., Jansen and Held, 2014) and be consistent with the model grid and damping parameters. The parameterized improvements, as suggested by the formal metrics of Fig. 5, may look insufficient, but this is only because the metrics is rather “tough”, as it penalizes not only for small-scale deviations but also for any misplacements of the eastward jet axis, which, perhaps, need no penalty. Visual inspection of the flow anomalies due to the

parameterization (Fig. 6) suggests that  $E_{rel}$  of about 30% implies that the parameterization restored nearly everything missing, and of about 50% implies that still most of the eastward jet and recirculations is actually recovered.

Finally, we implemented the parameterization in the common coarse-gridded models, which suffer also from the additional problems due to numerical errors (Fig. 7). The eddy viscosity values in these models are increased by an order of magnitude and also varied, in order to broadly assess performance of the eddy parameterization. The non-parameterized solutions are qualitatively similar to the corresponding

basic solutions from the equivalent coarse-grid models and lack the eastward jet and its recirculations in similar ways (not shown). Overall, on the grids  $257^2$  and  $129^2$ , the parameterization exhibits similar but slightly worse levels of improvement. Reducing eddy viscosity apparently helps, but not for  $\nu = 100 \text{ m}^2 \text{ s}^{-1}$  on the  $129^2$  grid, because this value is too small for capturing the viscous western boundary layer (Berloff and McWilliams, 1999) on the given grid. On the  $65^2$  grid the parameterization completely fails and shows absolutely no signs of improvement. All of these results and their counterparts with the equivalent grids suggest that local refinements of the grid and locally reduced eddy viscosity values in the eastward jet region are both beneficial for the parameterization performance. They also show that some reasonable level of the eddy activity is required by the parameterization, which is consistent with the fact that it amplifies the backscatter rather than completely emulates its effect.

In this section we systematically assessed performance of the proposed eddy parameterization and demonstrated its substantial utility for the purpose, by employing two types of models and considering a broad range of spatial grid resolutions and small-scale damping rate parameters. Thus, the scope of this paper — identifying large-scale flow anomalies due to the eddy backscatter, demonstrating that the backscatter can be controlled, and implementing the parameterization based on amplification of the backscatter — is completed, and in the next section we summarize and discuss its main findings.

## 6. Summary and discussion

This work continues development of dynamically consistent

parameterizations (Berloff, 2015; 2016) for representing mesoscale eddy effects in non-eddy-resolving and eddy-permitting ocean circulation models. We focused on the classical wind-driven double-gyre problem and on the main dynamic eddy effects that maintain the eastward jet extension of the western boundary currents and its adjacent recirculation zones via eddy backscatter mechanism. Despite its fundamental importance, this mechanism remains poorly understood and even dismissed, and in this paper we investigated it and, then, proposed its simple and efficient parameterization for use in eddy-permitting models.

We started by decomposing the reference eddy-resolving flow solution into the large-scale and eddy components defined by simple spatial filtering applied to each isopycnal layer of the ocean. Note, that this is a spatial scale-aware decomposition, rather than more common Reynolds decomposition into the time mean and fluctuations. The scale-aware approach is more relevant because it not only focuses on underresolved spatial scales, but also allows to consider correlations between the eddy scales and the evolving large scales, whereas the Reynolds decomposition tends to narrow dynamical analysis to the time-mean statistical balance. Most recently, scale-aware decompositions were applied for dynamical analyses of the comprehensive ocean circulation by Aluie et al. (2018).

Next, we find that the eastward jet and its recirculations are robustly present not only in the large-scale flow itself, but also in the rectified time-mean eddies, and in the transient rectified eddy component, which consists of highly anisotropic ribbons of the opposite-sign potential vorticity anomalies straddling the instantaneous eastward jet core and responsible for its persistent amplification. This transient

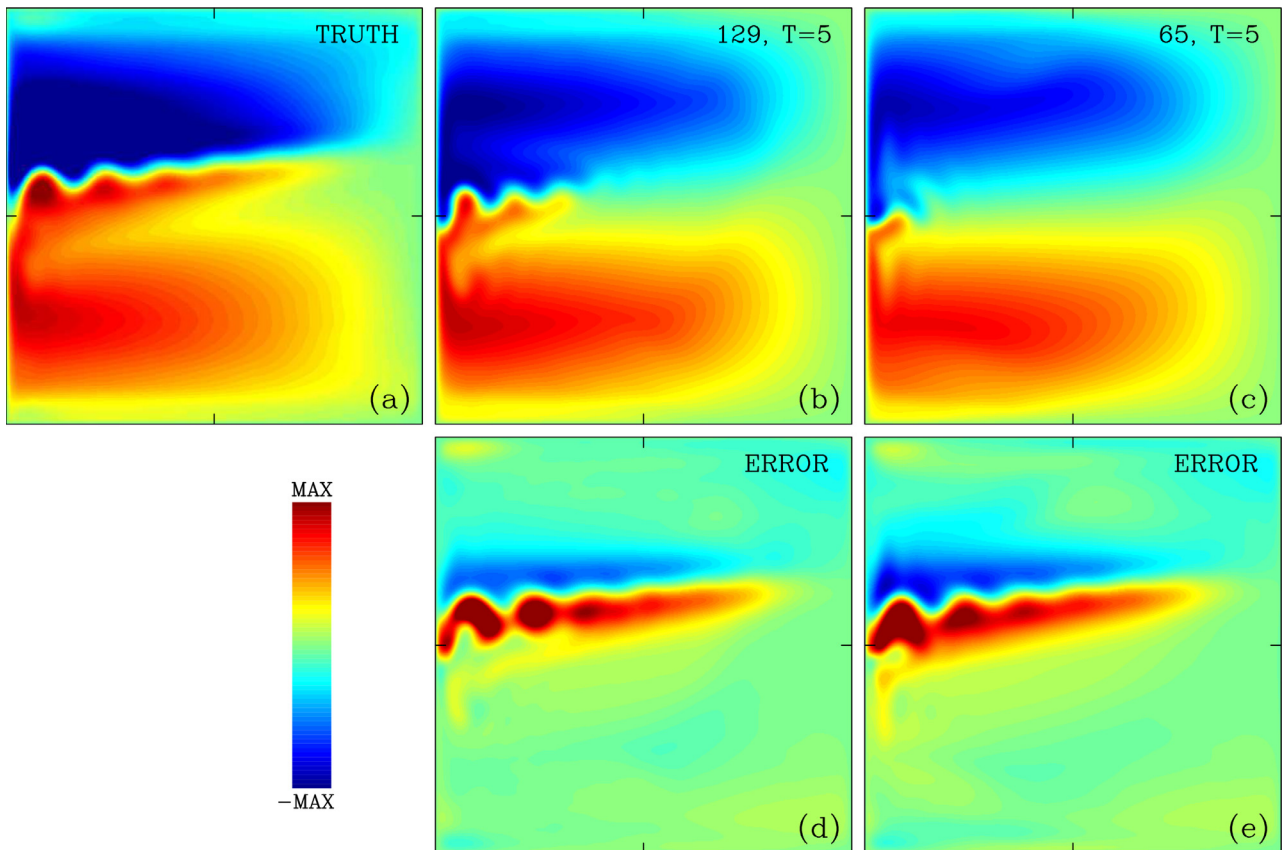


**Fig. 6.** Examples of the basic solutions without and with the implemented parameterization. It is clear that the parameterization substantially improves the solutions, and more so on the finer grid. Upper-layer time-mean velocity stream functions are shown, and all flow fields have the same but arbitrary units. The reference eddy-resolving solution is shown in (a), and two examples of the basic solutions correspond to  $T_i = 5$  days and equivalent grid resolutions (i.e., coarsenings) of (b)  $129^2$  and (c)  $65^2$ . Error fields, that is, differences between the reference solution and basic solutions in (b,c) are shown in the second row of panels: (d)  $129^2$ , (e)  $65^2$ . Third and fourth rows of panels show the parameterized solutions corresponding to (b) and (c), respectively: (f,i) time-mean flow fields (to be compared with (b) and (c), respectively); (g,j) flow anomalies induced by the parameterization on the top of the basic solutions; (h,k) error fields.

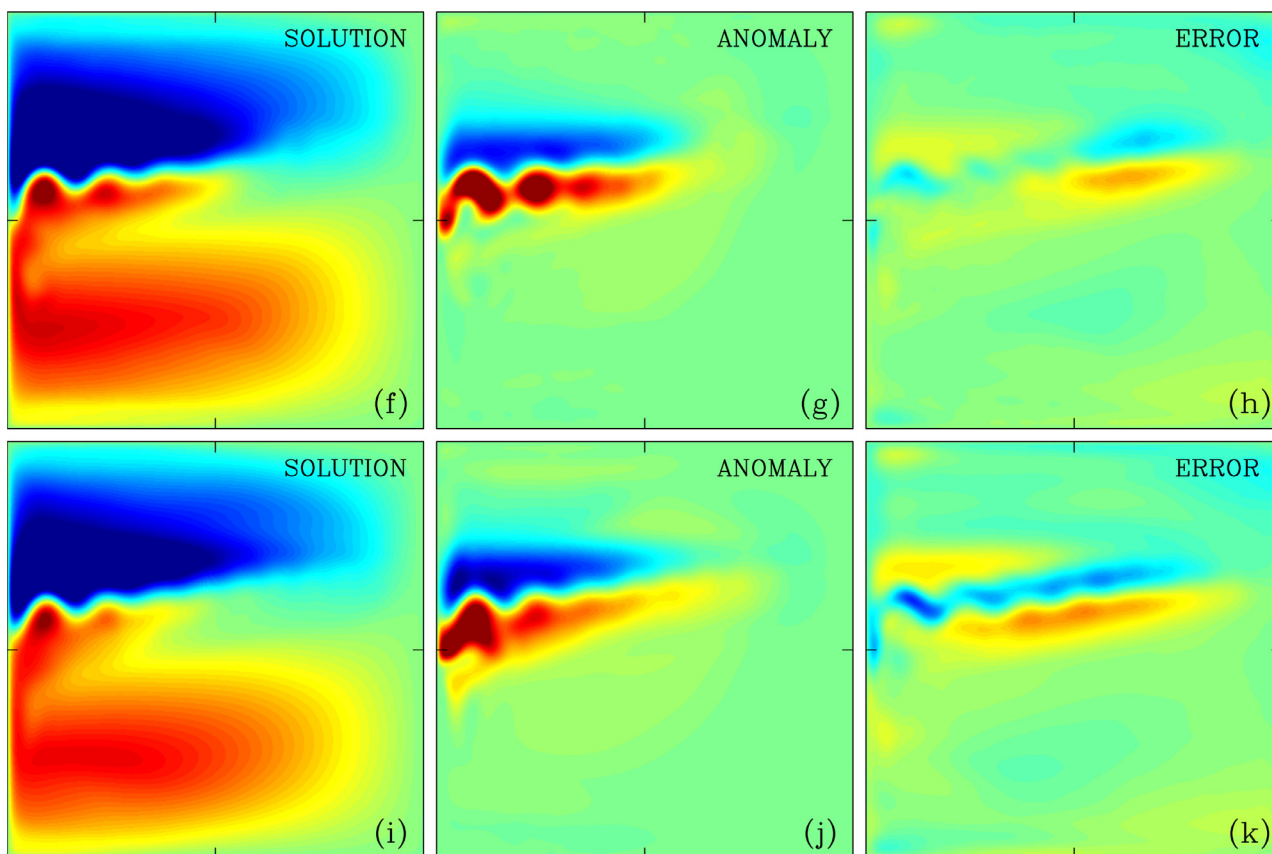


Fig. 6. (continued)

component is separated from the flow by the novel jet-following re-mapping method, in which the jet core is defined as the upper-ocean streamline that minimizes average magnitude of the relative vorticity along it. We hypothesize that all three components of the eastward jet are ultimately driven by the small-scale transient eddy forcing via the eddy backscatter mechanism, rather than by the mean eddy forcing and large-scale nonlinearities. This hypothesis is verified by progressively damping the backscatter and by observing the induced flow anomalies not only in the eddy field but, more importantly, in the large-scale component of the eastward jet and its recirculation zones.

The above analysis leads us to formulating the central eddy parameterization hypothesis: at least partially resolved eddy backscatter in an eddy-permitting model can be significantly amplified to improve the solution. Such amplification is a simple and novel eddy parameterization framework implemented here in terms of local, deterministic flow roughening controlled by single parameter. We test the parameterization skills in an hierarchy of non-eddy-resolving and eddy-permitting modifications of the original model and demonstrate, that indeed it can be highly efficient for restoring the eastward jet extension and its recirculations.

The new deterministic parameterization framework not only combines remarkable simplicity with good performance but also is dynamically transparent, therefore, it provides a powerful alternative to the common eddy diffusion and emerging stochastic parameterizations.

Our approach is conceptually similar but not identical to San et al. (2013), who proposed the approximate deconvolution technique<sup>3</sup>, to Jansen and Held (2014), who proposed injection of extra energy by negative viscosity affecting small but not the smallest (still

damped) resolved length scales, and to the studies that advocate use of stochastic small-scale forcing (e.g., Berloff, 2005b; Porta Mana and Zanna, 2014; Grooms et al., 2015b; and Zanna et al. (2017)). One way or another, explicitly or implicitly, all of the above approaches require a priori parametric decisions about length scales or patterns that are to be energized, as well as about their phases and amplitudes. The parameters involved can be spatially inhomogeneous and nonstationary, and their closures on the resolved large-scale fields can be elusive. The main novelties of our approach — backed up by systematic analyses of the eddy backscatter in the prototype model of the midlatitude wind-driven gyres — are the following: *determinism*, that is, no imposed stochasticity; maximal reliance on the resolved flow dynamics, that is, *dynamical consistency*; and minimal number of tunable parameters. Actually, the parameterization effectively involves only a single main parameter, which is the (negative) relaxation time. The secondary parameter is the spatial filter width, but once it is set to be several first baroclinic Rossby deformation radii (here,  $5R_{d1}$ ), its modest variations yield no significant sensitivities, as we found, beyond those that can be easily absorbed in retuning the relaxation time parameter. By no means we claim that our choice of the roughening operator is optimal, but it does the job and is very simple, therefore, it can be viewed as a good starting point for the algorithm.

Another somewhat technical but important aspect of our study is determining dependence of the relaxation time parameter on the nominal grid resolution. Indeed, a practical parameterization for use in eddy-permitting models should be resolution-aware — the more eddy scales are dynamically resolved and acting, the less should be contribution of the parameterization (e.g., Hallberg, 2013 proposed a simple functional dependence of parameters on the ratio between the first baroclinic Rossby deformation radius and the grid interval). We explored empirically the resolution awareness of the parameterization and showed that it can be dealt with by retuning the relaxation time. We demonstrated that, although finer grid resolution is always

<sup>3</sup> Effectively, Zanna et al. (2017) also proposed a deconvolution method, without actually acknowledging this. They introduced extra forcing parameterizing eddy effects by constructing the term with the Laplacian operator acting on the PV material derivative, but this is equivalent to roughening PV field by the elliptic differential filter (e.g., San et al., 2013).

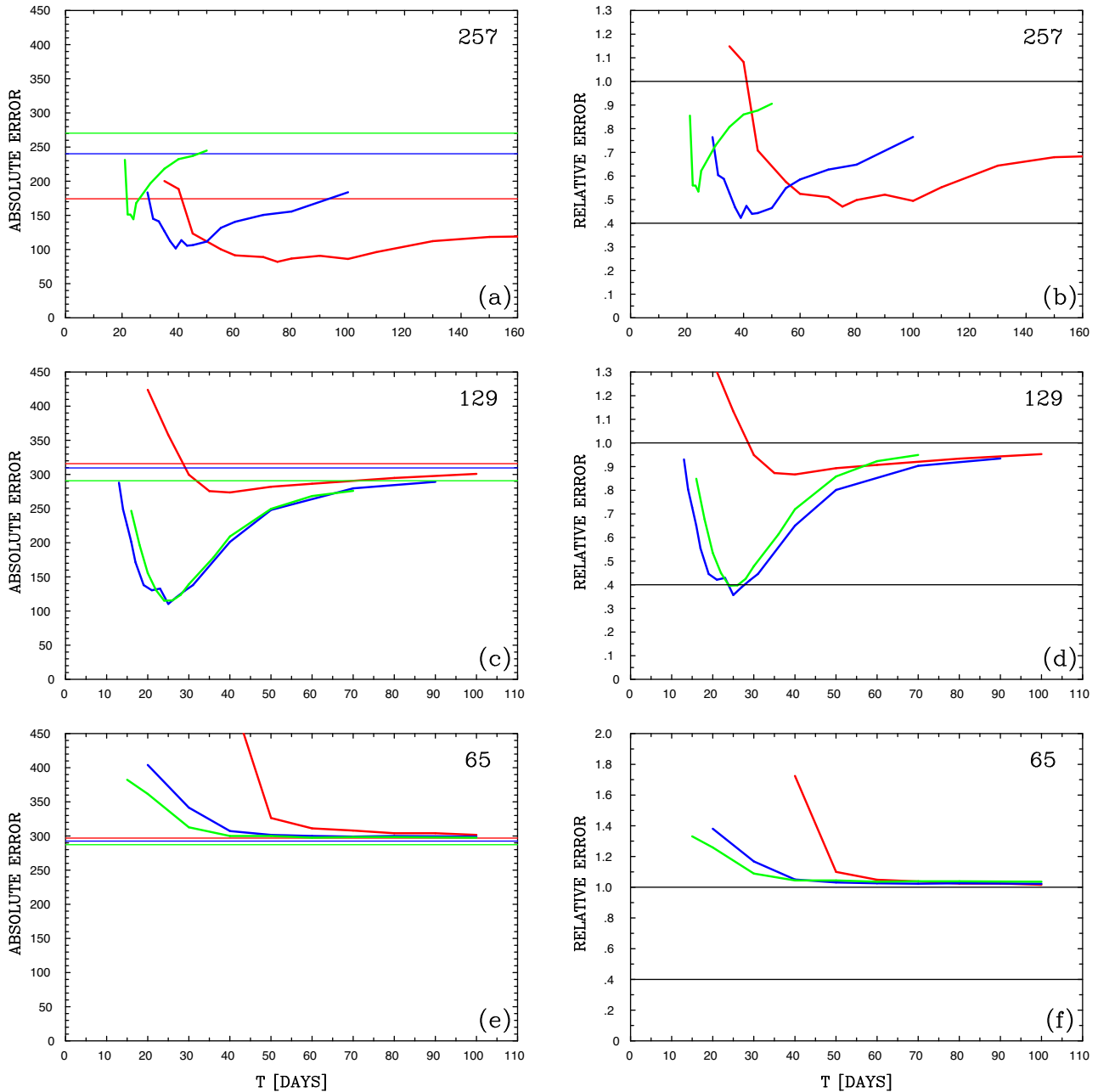


**Fig. 7.** Effect of the parameterization implemented in the coarse-grid models with the following actual grid sizes: (a,b)  $257^2$ , (c,d)  $129^2$ , (e,f)  $65^2$  grid points. Colours correspond to solutions with the following eddy viscosity values: (a–d) 100 (red), 200 (blue) and 400 (green)  $\text{m}^2 \text{s}^{-1}$ ; (e–f) 200 (red), 400 (blue) and 800 (green)  $\text{m}^2 \text{s}^{-1}$ . Horizontal straight (coloured) lines on the left panels indicate errors  $E_b$  of the coarse-grid nonparameterized solutions; all errors are given in terms of (arbitrary) nondimensional units, which are the same for all left panels. Curved (coloured) lines on the left panels show errors  $E$  of the parameterized (i.e., amplified) coarse-grid solutions, as functions of the amplification time  $T_a$ . Right panels show the corresponding relative error  $E_{rel} = E/E_{cg}$  curves, with all values normalized by the coarse-grid-solution error  $E_{cg}$ ; for convenience, the black horizontal lines indicate  $E_{rel}$  equal to unity and 0.4. Panels (e–f) show that the parameterization does not work for the  $65^2$ -grid solutions and performs poorly for  $\nu = 100 \text{ m}^2 \text{ s}^{-1}$  solution on the  $129^2$  grid. (For interpretation of the references to colour in this figure legend, the reader is referred to the web version of this article.)

beneficial for the parameterization accuracy, the parameterization itself has significant and positive impact, even when the grid interval is about  $Rd_1$ . For grids coarser than that, the proposed deterministic parameterization is not expected to work, because there is simply not enough eddy dynamics to be amplified, and some other approach has to be taken (e.g., Berloff, 2015).

The main future development of this work should be its extension from idealized process studies involving the quasigeostrophic approximation to the primitive equations routinely used in comprehensive OGCMs. The main task in the primitive equations will be transforming relatively simple roughening of the PV field into dynamically

consistent, simultaneous roughenings of the velocity, pressure and buoyancy fields. Other useful extensions should be studying effects of the deterministic parameterization on higher-order eddy statistics, beyond just comparing the time-mean fields, and on large-scale low-frequency variability of the gyres. Optimization and, perhaps, re-consideration of the roughening operator is also left for the future. Estimating and fitting spatially inhomogeneous relaxation time field would be another improvement. Finally, an obvious future extension is considering and parameterizing other eddy backscatters, beyond the eastward jet extension of the western boundary currents; this requires systematic analyses of other useful flow prototypes.

## Acknowledgments

This work was supported by the NERC grant NE/R011567/1 and Research Impulse grant DRI036PB. The author is grateful to the anonymous reviewers for their thoughtful and useful comments.

## References

- Aluie, H., Hecht, M., Vallis, G., 2018. Mapping the energy cascade in the north atlantic ocean: the coarse-graining approach. *J. Phys. Oceanogr.* 48, 225–244.
- Andrzejczak, M., Cooper, F., Juricke, S., Palmer, T., Weisheimer, A., Zanna, L., 2016. Oceanic stochastic parameterizations in a seasonal forecast system. *Mon. Weather Rev.* 144, 1867–1875.
- Anstey, J., Zanna, L., 2017. A deformation-based parametrization of ocean mesoscale eddy Reynolds stresses. *Ocean Model.* 112, 99–111.
- Berloff, P., 2005a. On dynamically consistent eddy fluxes. *Dyn. Atmos. Oceans* 38, 123–146.
- Berloff, P., 2005b. Random-forcing model of the mesoscale oceanic eddies. *J. Fluid Mech.* 529, 71–95.
- Berloff, P., 2015. Dynamically consistent parameterization of mesoscale eddies. Part I: simple model. *Ocean Model.* 87, 1–19.
- Berloff, P., 2016. Dynamically consistent parameterization of mesoscale eddies. part II: eddy fluxes and diffusivity from transient impulses. *Fluids* 1 (22). <http://dx.doi.org/10.3390/fluids1030022>.
- Berloff, P., Hogg, A., Dewar, W., 2007. The turbulent oscillator: a mechanism of low-frequency variability of the wind-driven ocean gyres. *J. Phys. Oceanogr.* 37, 2363–2386.
- Berloff, P., McWilliams, J., 1999. Quasigeostrophic dynamics of the western boundary current. *J. Phys. Oceanogr.* 29, 2607–2634.
- Berloff, P., McWilliams, J., 2003. Material transport in oceanic gyres. Part III: randomized stochastic models. *J. Phys. Oceanogr.* 33, 1416–1445.
- Buizza, R., Miller, M., Palmer, T., 1999. Stochastic representation of model uncertainties in the ECMWF ensemble prediction system. *Q. J. R. Met. Soc.* 125, 2887–2908.
- Chapman, C., 2014. Southern ocean jets and how to find them: improving and comparing common jet detection methods. *J. Geophys. Res.* 119, 4318–4339.
- Chen, R., Gille, S., McClean, J., Flierl, G., Griesel, A., 2015. A multi-wavenumber theory for eddy diffusivities and its application to the southeast pacific (DIMES) region. *J. Phys. Oceanogr.* 45, 1877–1896.
- David, T., Marshall, D., Zanna, L., 2017. The statistical nature of turbulent barotropic jets. *Ocean Model.* 119, 4318–4339.
- Delman, A., McClean, J., Sprintall, J., Talley, L., Yulaeva, E., 2015. Effects of eddy vorticity forcing on the mean state of the Kuroshio extension. *J. Phys. Oceanogr.* 45, 1356–1375.
- Duan, J., Nadiga, B., 2007. Stochastic parameterization for large eddy simulation of geophysical flows. *Proc. Am. Math. Soc.* 135, 1187–1196.
- Eden, C., 2011. A closure for meso-scale eddy fluxes based on linear instability theory. *Ocean Model.* 39, 362–369.
- Eden, C., Greatbatch, R., 2008. Towards a mesoscale eddy closure. *Ocean Model.* 20, 223–239.
- Frederiksen, J., O’Kane, T., Zidikheri, M., 2012. Stochastic subgrid parameterizations for atmospheric and oceanic flows. *Phys. Scr.* 85, 068202.
- Gent, P., McWilliams, J., 1990. Isopycnal mixing in ocean circulation models. *J. Phys. Oceanogr.* 20, 150–155.
- Grooms, I., 2016. A Gaussian-product stochastic Gent–McWilliams parameterization. *Ocean Model.* 106, 27–43.
- Grooms, I., Lee, Y., Majda, A., 2015b. Numerical schemes for stochastic backscatter in the inverse cascade of quasigeostrophic turbulence. *Multiscale Model. Simul.* 13, 1001–1021.
- Grooms, I., Majda, A., Smith, K., 2015a. Stochastic super parametrization in a quasigeostrophic model of the antarctic circumpolar current. *Ocean Model.* 85, 1–15.
- Hallberg, R., 2013. Using a resolution function to regulate parameterizations of oceanic mesoscale eddy effects. *Ocean Model.* 72, 92–103.
- Herring, J., 1996. Stochastic modeling of turbulent flows. In: Adler, R., et al. (Ed.), *Stochastic Modelling in Physical Oceanography*. Birkhauser, pp. 467.
- Ivchenko, V., Danilov, S., Schroter, J., 2014b. Comparison of the effect of parameterized eddy fluxes of thickness and potential vorticity. *J. Phys. Oceanogr.* 44, 2470–2484.
- Ivchenko, V., Danilov, S., Sinha, B., Schroter, J., 2014a. Integral constraints for momentum and energy in zonal flows with parameterized potential vorticity fluxes: governing parameters. *J. Phys. Oceanogr.* 44, 922–943.
- Jansen, M., Held, I., 2014. Parameterizing subgrid-scale eddy effects using energetically consistent backscatter. *Ocean Model.* 80, 36–48.
- Jansen, M., Held, I., Adcroft, A., Hallberg, R., 2015. Energy budget-based backscatter in an eddy permitting primitive equation model. *Ocean Model.* 94, 15–26.
- Juricke, S., Palmer, T., Zanna, L., 2017. Stochastic subgrid-scale ocean mixing: impacts on low-frequency variability. *J. Climate* 30, 4997–5019.
- Killworth, P., 1997. On the parameterization of eddy transfer. part i. theory. *J. Mar. Res.* 55, 1171–1197.
- Li, H., von Storch, J.S., 2013. On the fluctuating buoyancy fluxes simulated in a 1/10-degree OGCM. *J. Phys. Oceanogr.* 43, 1270–1287.
- Mak, J., Marshall, D., Maddison, J., Zanna, L., 2017. Emergent eddy saturation from an energy constrained eddy parameterisation. *Ocean Model.* 112, 125–138.
- McWilliams, J., 2008. The nature and consequences of oceanic eddies. In: Hecht, M., Hasumi, H. (Eds.), *Eddy-Resolving Ocean Modeling*. AGU Monograph, pp. 131–147.
- Porta Mana, P., Zanna, L., 2014. Toward a stochastic parameterization of ocean mesoscale eddies. *Ocean Model.* 79, 1–20.
- Ringler, T., Gent, P., 2011. An eddy closure for potential vorticity. *Ocean Model.* 39, 125–134.
- Rypina, I., Kamenkovich, I., Berloff, P., Pratt, L., 2012. Eddy-induced particle dispersion in the upper-ocean north atlantic. *J. Phys. Oceanogr.* 42, 2206–2228.
- San, O., Staples, A., Iliescu, T., 2013. Approximate deconvolution large eddy simulation of a stratified two-layer quasigeostrophic ocean model. *J. Phys. Oceanogr.* 63, 1–20.
- Shevchenko, I., Berloff, P., 2016. Eddy backscatter and counter-rotating gyre anomalies of midlatitude ocean dynamics. *Fluids* 1, 28. <http://dx.doi.org/10.3390/fluids1030028>.
- Smagorinsky, J., 1963. General circulation experiments with the primitive equations. i. the basic experiment. *Mon. Wea. Rev.* 91, 99–164.
- Starr, V., 1968. *Physics of negative viscosity phenomena*. McGraw-Hill, New York.
- Visbeck, M., Marshall, J., Haine, T., Spall, M., 1997. Specification of eddy transfer coefficients in coarse-resolution ocean circulation models. *J. Phys. Oceanogr.* 27, 381–401.
- Williams, P., Howe, N., Gregory, J., Smith, R., Joshi, M., 2016. Improved climate simulations through a stochastic parameterization of ocean eddies. *J. Climate* 29, 8763–8781.
- Zanna, L., Mana, P.P., Anstey, J., David, T., Bolton, T., 2017. Scale-aware deterministic and stochastic parametrizations of eddy-mean flow interaction. *Ocean Model.* 111, 66–80.
- Zhao, R., Vallis, G., 2008. Parameterizing mesoscale eddies with residual and Eulerian schemes, and a comparison with eddy-permitting models. *Ocean Model.* 23, 1–12.